Transactions, SMiRT-22
San Francisco, California, USA - August 18-23, 2013
Division V (include assigned division number from I to X)

VIBRATION CONTROL OF CIVIL STRUCTURES USING TUNED MASS DAMPERS WITH ADJUSTABLE STIFFNESS

Ging-Long Lin[1], Chi-Chang Lin[2], Bo-Cheng Chen[3]

[1] Post-Doctoral Research Fellow, Dept. of Civil Engineering, National Chung Hsing University, Taiwan
[2] Professor, Dept. of Civil Engineering, National Chung Hsing University, Taiwan
[3] Master, Dept. of Civil Engineering, National Chung Hsing University, Taiwan

ABSTRACT

The tuned mass damper (TMD) technique has been implemented in high-rise buildings, observatory towers, building floors, railway bridges and pedestrian bridges against natural and man-made loadings for near 40 years. TMDs can be incorporated into any structure with less interference compared with other energy dissipation devices. Although the design and application of traditional linear TMD systems are well developed, detuning effect and excessive stroke of TMD are the two major problems to be solved. In order to enhance the performance of TMD systems, some researchers have proposed a TMD with semi-active variable stiffness device (VSD). The VSD can be classified into on-off type VSD and continuous type VSD. The continuous VSD is effective in mitigating detuning effect while the on-off VSD is effective in reducing TMD stroke. In this study, a resettable variable stiffness TMD (RVS-TMD) is proposed to combine the advantages of the continuous and the on-off typed variable stiffness TMD. This study numerically simulates the dynamic behavior of a structural system controlled by the RVS-TMD, and compares its control performance with the optimal passive TMD and conventional variable stiffness TMD systems.

INTRODUCTION

Vibration control of civil engineering structures using tuned mass dampers (TMD) is a widely accepted control strategy after numerous analytical and experimental verifications (Lin *et al.* 2001). The TMD technique has been implemented in high-rise buildings, observatory towers, building floors, railway bridges and pedestrian bridges against natural and man-made loadings. Although the design and application of traditional linear TMD systems are well developed, there still remain two major problems associated with TMD systems to be solved, i.e. (1) detuning effect and (2) excessive stroke of TMD. The detuning effect occurs when TMD frequency does not tune to the desired value. The TMD stroke is large when the damping mechanism of the TMD is not efficient.

In order to improve the performance of TMD systems, some researchers have proposed a TMD with semi-active variable stiffness device (VSD). The VSD can be classified into two types: (1) on-off VSD (Chey *et al.* (2010)), and (2) continuous VSD (Nagarajaiah and Sonmez (2007); Lu *et al.* 2010). The continuous VSD is effective in mitigating detuning effect while the on-off VSD is effective in reducing TMD stroke. In this study, a resettable variable stiffness TMD (RVS-TMD) is proposed to combine the advantages of the continuous and the on-off typed variable stiffness TMD. The RVS-TMD is composed of a TMD and a resettable variable stiffness device (RVSD) which consists of a resettable element and a controllable stiffness element. By varying the stiffness element of RVSD, the detuning effect can be mitigated. While, by actuating the resettable element, the hysteresis loop of the RVSD can cover all four quadrants in the force-deformation diagram and thus result in more energy dissipation. The applicability and efficacy of RVS-TMD system for the protection of civil structures against earthquake loadings are investigated. Its control performance is also compared with those of the optimal passive TMD and the conventional variable stiffness TMD systems.

SYSTEM MODELING AND EQUATION OF MOTION

System Modeling

Fig. 1 shows a schematic diagram of a primary structure equipped with the RVS-TMD. The TMD is supported by a sliding platform, which consists of guide rails, sliding blocks and springs. The springs provide not only stiffness and resilience, but also a tuning frequency. Fig. 2 illustrates the overall mathematic model of Fig. 1. The figure shows that the sliding platform of the RVS-TMD is modeled by a spring of stiffness k_s and a friction element with friction coefficient μ_f. The former simulates stiffness due to the resilient mechanism whereas the latter models the friction effect of the guide rail of the sliding platform. The mass of the RVS-TMD and the primary structure are denoted by m_s and m_p, respectively. Moreover, the damping and stiffness of the primary structure are denoted by c_p and k_p, respectively. Relative-to-the-ground displacements of the RVS-TMD and the primary structure are denoted by x_s and x_p , respectively. Moreover, as shown in Fig. 3(a), the RVSD itself consists of a variable stiffness and a resettable device. Symbol $u_d(t)$ and $k_d(t)$ denote the force and controllable stiffness of the RVSD, respectively; $d_e(t)$ represents the elongation of the variable stiffness; and $d_s(t)$ denotes the displacement of the resettable device. If $k_d(t)$ is a constant in the RVSD, it becomes a conventional on-off type VSD, or called resetting semi-active stiffness device (RSASD) (Yang *et al.* 2000), as shown in Fig. 3(b). With a constant k_d in Fig. 2, the RVS-TMD system becomes a RSAS-TMD system. Based on the mathematical model in Fig. 2, the dynamic equation of the RVS-TMD system can be rewritten as

$$\mathbf{M}\ddot{\mathbf{x}}(t)+\mathbf{C}\dot{\mathbf{x}}(t)+\mathbf{K}\mathbf{x}(t)=\mathbf{D}_2(u_f(t)+u_d(t))+\mathbf{E}\ddot{x}_g(t) \tag{1}$$

where

$$\mathbf{x}(t)=\begin{Bmatrix}x_p(t)\\ v_s(t)\end{Bmatrix},\quad \mathbf{D}_2=\begin{Bmatrix}1\\ -1\end{Bmatrix},\quad \mathbf{E}_1=\begin{Bmatrix}-m_p\\ -m_s\end{Bmatrix},\quad \mathbf{M}=\begin{bmatrix}m_p & 0\\ m_s & m_s\end{bmatrix},\quad \mathbf{C}=\begin{bmatrix}c_p & 0\\ 0 & 0\end{bmatrix},\quad \mathbf{K}=\begin{bmatrix}k_p & -k_s\\ 0 & k_s\end{bmatrix} \tag{2}$$

In Eq. (2), **x**(t) denotes the vector containing the system responses consisting of structural displacement $x_p(t)$ and TMD stroke $v_s(t)$; $\ddot{x}_g(t)$ is the ground acceleration due to an earthquake; $\mathbf{D}_2$ and $\mathbf{E}_1$ denote the force placement matrices for the RVS-TMD system and the excitation, respectively. The matrices **M**, **C** and **K** represent the mass, damping and stiffness matrices of the RVS-TMD control system, respectively. The friction force of the sliding platform are denoted by $u_f(t)$. Moreover, the forces denoted by $u_d(t)$ and $u_f(t)$ on the right-hand side of Eq. (1) are the nonlinear force effects of the RVS-TMD. Note that $u_d(t)$ is the resettable device force, $u_f(t)$ is a friction force. Therefore, the dynamic response of the RVS-TMD system can be attenuated by altering the device force $u_d(t)$ in real time.

Furthermore, for the convenience of the later numerical analysis, the dynamic equation shown in Eq.(1) is recast in a state space form, i.e.,

$$\dot{\mathbf{z}}(t)=\mathbf{A}\,\mathbf{z}(t)+\mathbf{B}\,(u_d(t)+u_f(t))+\mathbf{E}\,\ddot{x}_g(t) \tag{3}$$

where the state vector **z**(*t*), the system matrix **A** and the force placement matrices **B** and **E** can be written explicitly as

$$\mathbf{z}(t)=\begin{bmatrix}\mathbf{x}(t) & \dot{\mathbf{x}}(t)\end{bmatrix}^T=\begin{bmatrix}x_p(t) & v_s(t) & \dot{x}_p(t) & \dot{v}_s(t)\end{bmatrix}^T \tag{4}$$

$$\mathbf{A}=\begin{bmatrix}\mathbf{0} & \mathbf{I}\\ -\mathbf{M}^{-1}\mathbf{K} & -\mathbf{M}^{-1}\mathbf{C}\end{bmatrix},\quad \mathbf{B}=\begin{bmatrix}\mathbf{0}\\ \mathbf{M}^{-1}\mathbf{D}_2\end{bmatrix},\quad \mathbf{E}=\begin{bmatrix}\mathbf{0}\\ \mathbf{M}^{-1}\mathbf{E}_1\end{bmatrix} \tag{5}$$

For the purpose of numerical simulation, the Coulomb friction law is assumed to govern friction material behavior in the sliding platform, and the friction materials are assumed to have an equal static and dynamic friction coefficient.

Mass Ratio and Tuning Frequency Ratio

In this study, mass ratio of the TMD system is defined as

$$\mu = m_s / trace(\mathbf{m}_p) \tag{6}$$

where *trace*(**x**) is the sum of diagonal elements of **x**. For design purposes, Lin *et al*. (1994) presented the optimal passive TMD parameters via simple equations using the regression method. The equations of optimal tuning frequency ratio, R_s, and damping ratio, ζ_s, for structures are defined as follows

$$R_{s,opt} = f_s / f_p = [a/(1+\mu)]^b; \quad a = 1.0 - \xi_p / 4, \quad b = 1.35 e^{3.2\xi_p} \tag{7}$$

$$\xi_{s,opt} = 0.46\mu^{0.48} \tag{8}$$

where f_s and f_p represent the frequency of the TMD and primary structure, respectively. ζ_s and ζ_p denote the damping ratio of the TMD and primary structure, individually. In this study, for the resettable TMD systems, damping is provided by the resettable device; therefore, Eq. (7) is utilized to determine the optimal tuning frequency, and Eq. (8) is only used for comparing the optimal passive TMD with the resettable TMD systems.

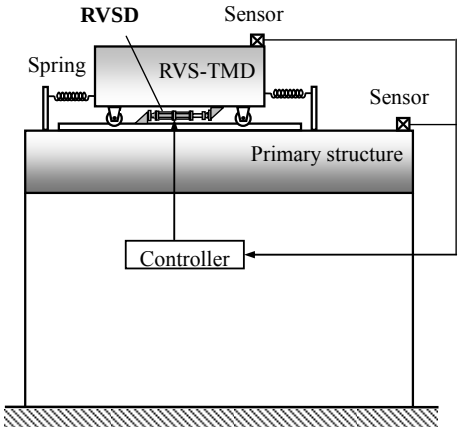

Figure 1 Schematic diagram of a primary structure controlled by a RVS-TMD.

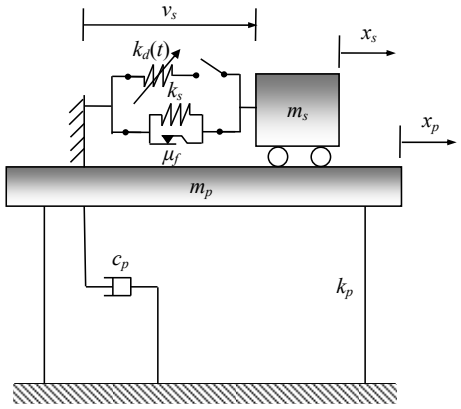

Figure 2 Mathematical model of a primary structure controlled by a RVS-TMD.

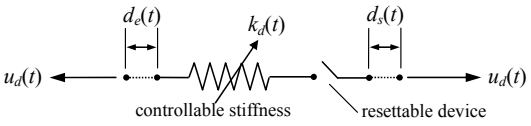

(a) Resettable Variable Stiffness Device (RVSD)

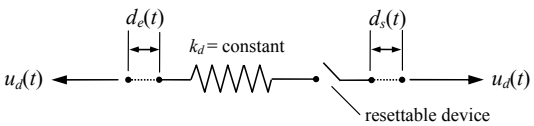

(b) Resetting Semi-active stiffness Device (RSASD)

Figure 3 Mathematical models.

Discrete-Time State-Space Equation

For simulation purpose, the discrete-time solution of Eq. (3) can be written in an incremental form.

$$\mathbf{z}[k+1] = \mathbf{A}_d\, \mathbf{z}[k] + \mathbf{B}_d\, (u_d[k] + u_f[k]) + \mathbf{E}_d\, \ddot{x}_g[k] \tag{9}$$

$$\mathbf{A}_d = e^{\mathbf{A}\Delta t}, \quad \mathbf{B}_d = \mathbf{A}^{-1}(\mathbf{A}_d\text{-}\mathbf{I})\,\mathbf{B}, \quad \mathbf{E}_d = \mathbf{A}^{-1}(\mathbf{A}_d\text{-}\mathbf{I})\,\mathbf{E} \tag{10}$$

Eq. (9) is also called the discrete-time state-space equation. In the equation, the coefficient matrices $\mathbf{A}_d$, $\mathbf{B}_d$, and $\mathbf{E}_d$ are all constant. In addition, Δt denotes the time interval (sampling period) for analysis. Inspecting Eq. (9) reveals that the next time-step response $\mathbf{z}[k+1]$ can be computed based on the state $\mathbf{z}[k]$, excitation $w[k]$, sliding platform friction force $u_f[k]$, and RVSD force $u_d[k]$, which are all evaluated at $u_d[k]$ the current time step, i.e., the k-th step. Note that $\mathbf{z}[k]$ may be computed from the previous (k-1)th step response by using Eq. (9) recursively, but $u_f[k]$ and $u_d[k]$ are both unknown nonlinear forces at the beginning of the k-th step and require special numerical treatment.

CONTROL OF THE RVSD

By controlling the variable stiffness, the RVSD force can follow a target force that is determined on-line by well developed active control laws. To this end, the control algorithm is divided into two parts below.

Control of the Controllable Stiffness Element

The RVSD also has a variable stiffness element $k_d[k]$, which can be varied on-line. A semi-active control law is employed for the determination of $k_d[k]$of the RVSD. Based on this control law, the idea stiffness $\hat{k}_d[k]$ at a certain time instant is computed by

$$\hat{k}_d[k] = \hat{u}_d[k] / d_e[k] \tag{11}$$

where
$$d_e[k] = \mathbf{D}_0\mathbf{z}[k] - d_s[k] = \mathbf{D}_0\mathbf{z}[k] - d_s[k-1] \tag{12}$$

$\hat{u}_d[k]$ is a target RVSD force that will be introduced below. After physical constraints are imposed, the control command for the stiffness $k_d[k]$ of the RVSD can be written as

$$k_d[k] = \begin{cases} k_{d,\min}, & for \quad \hat{k}_d[k] \le k_{d,\min} \\ \hat{k}_d[k], & for \quad k_{d,\min} < \hat{k}_d[k] < k_{d,\max} \\ k_{d,\max}, & for \quad \hat{k}_d[k] \ge k_{d,\max} \end{cases} \tag{13}$$

where $k_{d,min}$ and $k_{d,max}$ denote the physical lower and upper bounds of the variable stiffness, respectively, which must satisfy $k_{d,\max} \ge k_{d,\min} \ge 0$. It is worth mentioning that if the variable stiffness $k_d[k]$ of an RVSD becomes a constant, (i.e., $k_d[k] = k_d$), the RVSD will behave like a RSASD. In Eq. (11), the target control force, $\hat{u}_d[k]$, is determined using the direct output feedback control algorithm.

$$\hat{u}_d[k] = \mathbf{G}\,\mathbf{y}[k] = \begin{bmatrix} G_d & G_v \end{bmatrix} \begin{Bmatrix} v_s[k] \\ \dot{v}_s[k] \end{Bmatrix} = G_d v_s[k] + G_v \dot{v}_s[k] \tag{14}$$

where **G** is control gain, vector including displacement gain, G_d, and velocity gain, G_v. Displacement gain is used to adjust the stiffness of the RVSD, while velocity gain provides viscous damping for the RVSD. Both stiffness and damping of the RVS-TMD system can be adjusted by adjusting the target control force, $\hat{u}_d[k]$. Therefore, with appropriate control gains, the detuning effect can be avoided and the TMD stroke can be reduced. To optimally tune the natural frequency of the primary structure, the sum of k_s and G_d is

$$k_s + G_d = k_{s,opt} \tag{15}$$

Moreover, G_d can be adjusted to retune the RVS-TMD when structure stiffness changes. The following control algorithm is developed to retune the stiffness of the RVS-TMD.

If $0.95 f_p < f_p^{id} < 1.05 f_p$, then

$$G_d = k_{s,opt} - k_s \tag{16}$$

If $f_p^{id} < 0.95 f_p$ or $f_p^{id} > 1.05 f_p$, then $k_{s,opt}^{retune}$ is re-computed by Eq. (7) based on the identified f_p^{id}, and

$$G_d = k_{s,opt}^{retune} - k_s \tag{17}$$

where f_p^{id} is the identified natural frequency of the primary structure. Notably, G_d must be positive. Because the duration of an earthquake is short, retuning the stiffness of the RVS-TMD during an earthquake is difficult. The natural frequency of the primary structure can be identified from vibration records of the structures under wind, earthquake, or ambient excitation, such that stiffness adjustments can be performed offline. In Eq. (14), velocity gain, G_v, is determined by the linear-quadratic regulator (LQR) control algorithm, with direct output feedback (Chu *et al.* 2008). With an appropriate velocity gain, active control can produce an ellipse-like hysteretic loop and exhibit velocity-dependent damping.

Control of the Resettable Element

The control law for the resettable element is derived based on Lyapunov theory (Yang *et al.* 2000) and can be expressed as follows.

$$\text{If } \dot{v}_s[k]=0\text{, let } d_e[k]=0 \ (u_d[k]=0 \text{ and } d_s[k]=v_s[k]) \tag{18}$$

Eq. (18) resets RVSD stiffness at each moment when relative velocity, $\dot{v}_s[k]$, is zero. Resetting releases the accumulated vibration energy captured and stored in the constant stiffness component of the RVSD. Nevertheless, in order to avoid the opposite direction of current RVSD force and target force. The following disconnection command is defined as

$$\text{If } \hat{u}_d[k]\dot{v}_s[k]<0\text{, let } d_e[k]=0 \ (u_d[k]=0 \text{ and } d_s[k]=v_s[k]) \tag{19}$$

Eq. (19) is very simple because it does not require exact values for $\hat{u}_d[k]$ and $\dot{v}_s[k]$, only their signs. Implementation of this control method requires measurement of some selected structural responses $\mathbf{y}[k]$, as well as the TMD relative velocity, $\dot{v}_s[k]$. Fig. 4 shows the control block diagram of the proposed control method for an RVS-TMD system. It is worth mentioning that for a RSASD, k_d is a constant, only Eq. (18) is used to control the resettable element. It means the control algorithm of the RSASD is simpler. However, the control algorithm of the RVSD can be more flexible.

HYSTERETIC BEHAVIOR AND HARMONIC RESPONSE

To study the hysteretic behavior of the resettable TMD systems, a single degree-of-freedom (SDOF) system equipped with different resettable TMD under a harmonic load is investigated in this section.

System Parameters

Table 1 lists the numerical values of the SDOF system parameters, TMD system, and VSDs. The natural frequency and damping ratio of the primary structure are 1.0 Hz and 1.0%, respectively. The mass ratio, μ, is taken as 2% of the weight of the structure. The TMD frequency, f_s =0.98 Hz, is computed by Eq. (7). The friction coefficient of the sliding platform is taken to be μ_f=0.005 to simulate the low friction of linear guide way system. The control parameters for a RVSD include $k_{d,min}$ and $k_{d,max}$, which are usually determined by the physical constraint of the mechanism that produces variable stiffness. Suitable values of $k_{d,min}$ and $k_{d,max}$, the weighting matrices **Q** and R used in the LQR control, and the resulting gain matrix **G** are also listed in Table 1.

Table 1 System parameters for simulation.

System	Item	Value
Primary structure	Mass (m_p)	18,000 kg
	Frequency (f_p)	1.0 Hz
	Damping ratio (ζ_p)	1.0 %
TMD	Mass ratio (μ)	2.0 %
	Frequency (f_s)	0.9694 Hz
	Stiffness (k_s=$k_{s,opt}$)	13,355 N/m
	Friction coefficient (μ_f)	0.005
RSASD	Spring stiffness (k_d)	$k_d = 0.2k_{s,opt}$ ($k_s = 0.8k_{s,opt}$; $k_d + k_s = k_{s,opt}$)
RVSD	Max. RVSD stiffness ($k_{d,\max}$)	0.6 $k_{s,opt}$
	Min. RVSD stiffness ($k_{d,\min}$)	0.1 $k_{s,opt}$
	LQR weighting matrices	$\mathbf{Q}=\begin{bmatrix}\mathbf{I} & \mathbf{0}\\ \mathbf{0} & \mathbf{0}\end{bmatrix}$, $R=10^{-7}$
	Feedback gain matrix	$\mathbf{G}$ = [0.2$k_{s,opt}$ 569.72]

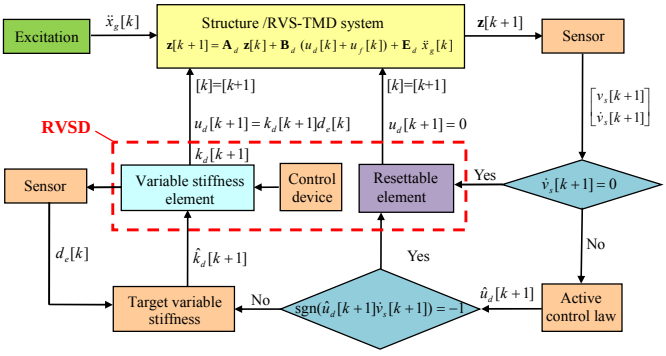

Figure 4 Control flowchart of the RVS-TMD system.

Harmonic Responses

Figure 5 shows the hysteresis loops of both VSDs when the structure-TMD systems are subjected to a harmonic ground acceleration of a frequency 1.0 Hz and amplitude 0.03g. Fig. 5(a) shows the RVSD is

able to closely follow the target force, which is determined by the LQR algorithm. In the Fig. 5(b), it is shown that the RSASD has hysteresis parallelogram loops, and the slope of the inclined straight-line segments in a parallelogram represents the constant damper stiffness k_d. Fig. 5 demonstrates that because of the resetting actions, the hysteresis loops of the RVSD and RSASD cover all four quadrants of the hysteretic diagrams. If the resetting function is removed, the hysteresis loops produced by a stiffness device can only exist in the first and third quadrants of the hysteretic diagrams (Lu and Lin 2009).

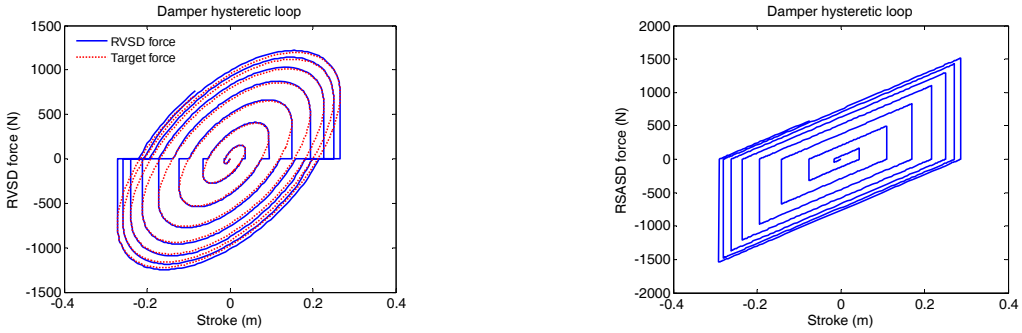

(a) RVSD (b) RSASD

Figure 5 Hysteresetic loops of the RVSD and the RSASD.

In order to verify the control algorithm of both VSDs, the time histories of the relative velocity, TMD stroke $v_s(t)$, spring elongation $d_e(t)$, resetting displacement $d_s(t)$, and device force $u_d(t)$ of the RSAS-TMD and RVS-TMD systems are all plotted in Fig. 6. It is evident that: (1) Both RVSD and RSASD are reset at each moment when the TMD velocity is equal to zero. (2) The sum of $d_s(t)$ and $d_e(t)$ is equal to $v_s(t)$. (3) A disconnection interval appears at each moment after resetting action. The directions of current RVSD force and target force are opposite in this interval. (4) The RSASD is reset at the moment of maximum device force in each cycle.

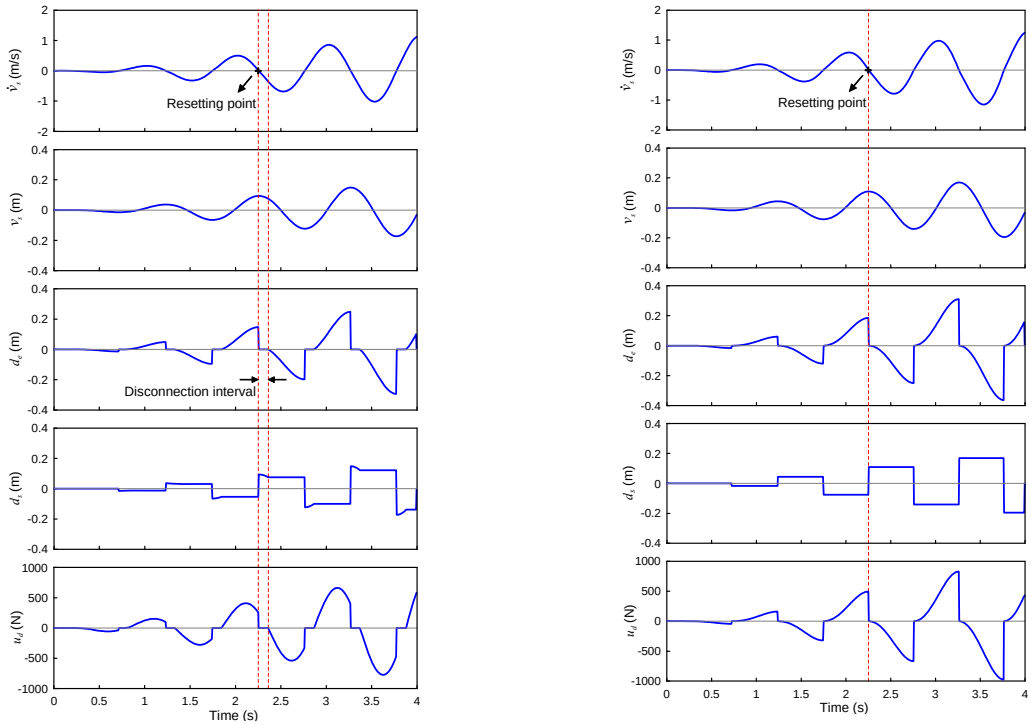

(a) RVSD (b) RSASD

Figure 6 Harmonic responses of the RVS-TMD and the RSAS-TMD systems.

Frequency Responses

In this subsection, the frequency responses of the RVS-TMD and RSAS-TMD system are investigated and compared. In order to do so, a harmonic ground acceleration of the form: $\ddot{x}_g(t) = 0.03g\sin(2\pi\,\beta_f\,f_p\,t)$, where f_p (=1.0Hz) denotes the frequency of the primary structure, and β_f represents the frequency ratio of the ground excitation, which is a variable defined as $\beta_f = f_g / f_p$, with f_g being the ground frequency. When the excitation frequency ratio β_f is varied from 0.8 to 1.2, Fig. 7 compares, respectively, the vibration amplitudes of the structural displacement and the TMD stroke for three types of TMD systems. These three types of TMD are the RVS-TMD, RSAS-TMD, and optimal passive TMD (PTMD) systems. Here, the vibration amplitudes mean the amplitudes of the steady-state responses of the systems. From Fig. 7, it is observed that for the uncontrolled structure, structural displacement has an obvious resonant peak when the frequency ratio β_f is close to one (i.e., the excitation frequency f_g is close to the structural frequency f_p). On the other hand, the resonance behavior is effectively attenuated in the RSAS-TMD, the RVS-TMD, and the PTMD cases. This implies that both variable stiffness TMD systems and PTMD are able to eliminate the severe resonance response.

One advantage of the proposed RVS-TMD is its ability to alleviate the detuning effect. We assume stiffness of the controlled primary structure is decreased by 15%. In this scenario, structural frequency changes by > 5%. Therefore, displacement gain, G_d, of the RVS-TMD is recomputed by Eq. (17). Fig. 8 shows that the detuning effect is markedly mitigated by introducing displacement gain, G_d, into the RVS-TMD system. Therefore, system robustness is enhanced. However, unlike an active device, the retuning action is achieved by adjusting the variable stiffness of the RVSD.

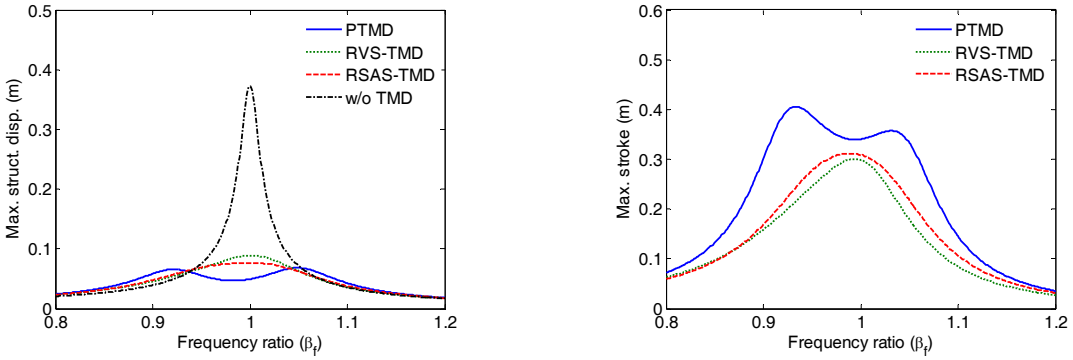

(a) Structural displacement (b) TMD stroke

Figure 7 Amplitude of steady-state response vs. excitation frequency.

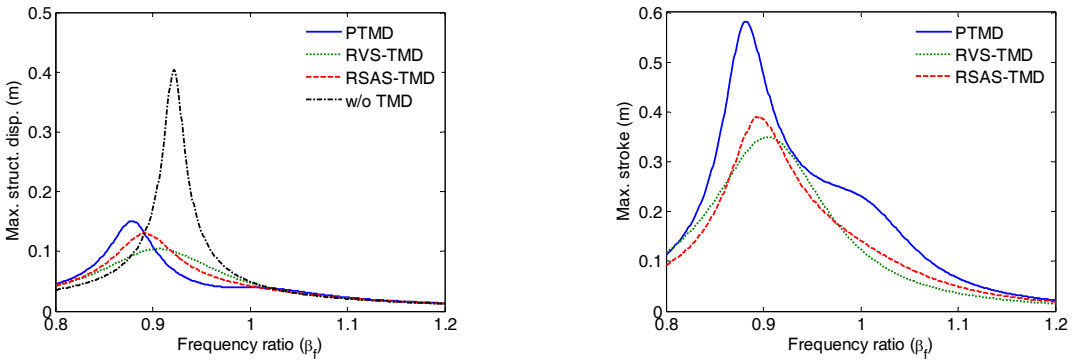

(a) Structural displacement (b) TMD stroke

Figure 8 Detuning effect on different TMD systems (15% stiffness reduction of the primary structure).

COMPARISON OF SEISMIC RESPONSES

Ground Acceleration Records for Simulation

Four ground accelerations with different characteristics are imposed on the above structural system. The properties of the four seismic events are: Mexico (f_g=ω_g/2π=0.5 Hz; ξ_g=0.3), Hachinohe (f_g=ω_g/2π=1.0 Hz; ξ_g=0.6), El Centro (f_g=ω_g/2π=1.9 Hz; ξ_g=0.6) and Kobe (f_g=ω_g/2π=1.9 Hz; ξ_g=0.3). Based on the Kanai-Tajimi spectra, the Mexico earthquake occurred on soft soil, and the energy was concentrated in a very narrow band around 0.5 Hz. Both the Hachinohe and the El Centro earthquakes were wide-band earthquakes with characteristic frequencies of 1.0 and 1.9 Hz, respectively. The Kobe earthquake was a narrow-band earthquake with a characteristic frequency of 1.9 Hz. Because of the natural frequency (f_p) of the SDOF structure is 1.0 Hz, the selected ground motions represent four different properties with respect to the SDOF structure: (1) Mexico ($f_p > f_g$, narrow-band), (2) Hachinohe ($f_p = f_g$, wide-band), (3) El Centro ($f_p < f_g$, wide-band) and (4) Kobe ($f_p < f_g$, narrow-band). In addition, a wide-band earthquake with $f_p > f_g$ is very few in nature.

Parametric Study

In order to quantify the control performance, the peak and RMS (root mean square) seismic responses of the RVSD and RSASD systems are evaluated. Six performance indices (J_1 to J_6) defined in Table 2 are employed. Fig. 9 depicts J_3 and J_5 of the RVS-TMD system as functions of control parameter R. The PGA (peak ground acceleration) of the four earthquakes has been scaled to 0.4g. From Fig. 9, it is evident that the RMS structural displacement decreases as R increases. However, the TMD stroke increases as R increases. From the above observations it may be concluded that for an RVS-TMD system, R =10^{-7} is a suitable value for a tradeoff between control performance and TMD stroke. This value will be used in the next section.

Table 2 Definition of performance indices.

Response	Peak structural displacement	Peak structural acceleration	Peak TMD stroke
Index	$J_1 = \dfrac{\max(x_p(t))_{w/\ TMD}}{\max(\bar{x}_p(t))_{w/o\ TMD}}$	$J_2 = \dfrac{\max(\ddot{x}_{p,a}(t))_{w/\ TMD}}{\max(\ddot{\bar{x}}_{p,a}(t))_{w/o\ TMD}}$	$J_5 = \max(v_s(t))$
Response	**RMS structural displacement**	**RMS structural acceleration**	**Peak device force**
Index	$J_3 = \dfrac{RMS(x_p(t))_{w/\ TMD}}{RMS(\bar{x}_p(t))_{w/o\ TMD}}$	$J_4 = \dfrac{RMS(\ddot{x}_{p,a}(t))_{w/\ TMD}}{RMS(\ddot{\bar{x}}_{p,a}(t))_{w/o\ TMD}}$	$J_6 = \max(u_d(t))$

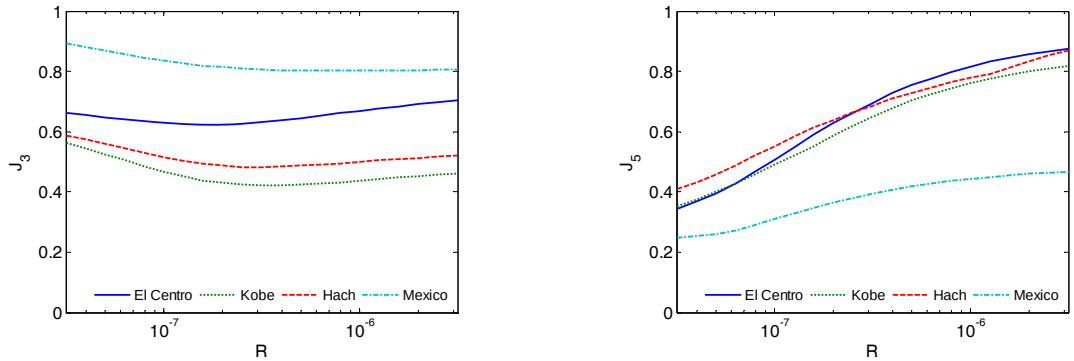

(a) J_3 (RMS structure disp.) (b) J_5 (Max. TMD stroke)

Figure 9 Parametric study of RVS-TMD (PGA=0.4g).

In order to select a suitable k_d for the RSAS-TMD system to be used in the later comparative study, Fig. 10 depicts the performance indices J_3 and J_5 as the functions of k_d, when the RSAS-TMD is subjected to

the four earthquakes mentioned above. In the figure, the damper stiffness k_d has also been normalized with respect to $k_{d,opt}$. From Fig. 10, it is evident that a stiffer k_d leads to a smaller TMD stroke, but a better control performance. For the convenience of comparison, a value of k_d =0.2$k_{d,opt}$ is chosen for the RSAS-TMD system in the later simulation.

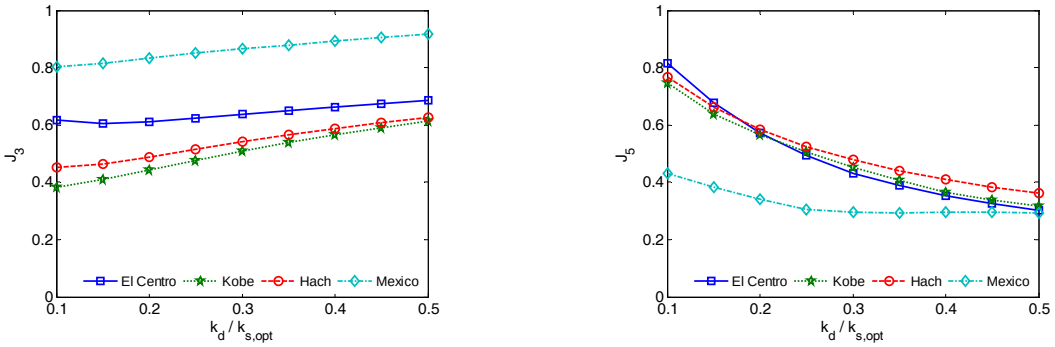

(a) J_3 (RMS structure disp.) (b) J_5 (Max. TMD stroke)

Figure 10 Parametric study of RSAS-TMD (PGA=0.4g).

Discussion on Seismic Control Performance

In order to quantify the control performance, the performance indices J_1 to J_6 of the RVS-TMD and RSAS-TMD systems are evaluated in this subsection. Control parameters of both TMD systems are listed in Table 1. Tables 3 and 4 summarize the six performance indices of the RVS-TMD and RSAS-TMD systems subjected to the four chosen earthquakes (PGA=0.4g). It is evident that both TMD systems are able to reduce structural responses caused by the earthquakes. The control performance of the RVS-TMD is similar to those of the RSAS-TMD with a smaller device force (J_6).

Table 3 Performance indices of the RVS-TMD system (PGA=0.4g).

Earthquake	Response Index				Stroke Index	Force Index
	J_1	J_2	J_3	J_4	J_5	J_6
El Centro	0.8046	0.7867	0.6165	0.6052	0.5920 m	2201 N
Kobe	0.9111	0.9049	0.4292	0.4217	0.5486 m	2018 N
Hachinohe	0.5592	0.5438	0.4893	0.4761	0.6194 m	2232 N
Mexico	0.7451	0.7159	0.8391	0.8155	0.3429 m	1119 N
Average	0.7550	0.7378	0.5935	0.5796	0.5257 m	1892 N

Table 4 Performance indices of the RSAS-TMD system (PGA=0.4g).

Earthquake	Response Index				Stroke Index	Force Index
	J_1	J_2	J_3	J_4	J_5	J_6
El Centro	0.8063	0.8045	0.6122	0.6113	0.5713 m	3014 N
Kobe	0.9117	0.9124	0.4424	0.4426	0.5675 m	2927 N
Hachinohe	0.5575	0.5536	0.4881	0.4851	0.5827 m	3103 N
Mexico	0.7520	0.7390	0.8325	0.8124	0.3405 m	1719 N
Average	0.7569	0.7524	0.5938	0.5879	0.5155 m	2691 N

Moreover, the proposed RVS-TMD is able to alleviate the detuning effect. When stiffness of the controlled primary structure is decreased by 15%, Fig. 11 shows the control performance of the RVS-TMD is better than those of the RSAS-TMD with a smaller TMD stroke.

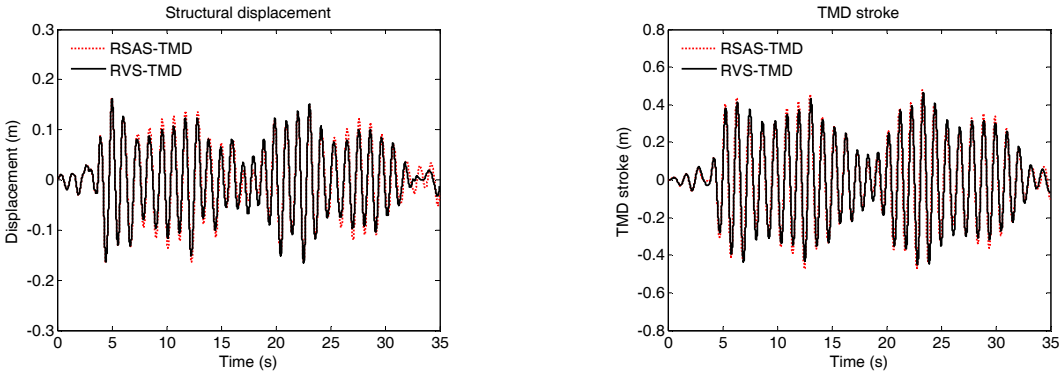

(a) Structural displacement (b) TMD stroke

Figure 11 Detuning effect (15% stiffness reduction of the primary structure).

CONCLUSION

In this study, a resettable variable stiffness TMD (RVS-TMD) is proposed to combine the advantages of the continuous and the on-off typed variable stiffness TMD. By varying the stiffness element of RVSD, the detuning effect can be mitigated. While, by actuating the resettable element, the hysteresis loop of the RVSD can result in more energy dissipation. A parametric study is investigated to find the optimal control parameters. Compared with the conventional variable stiffness TMD, it is evident that the proposed RVS-TMD can alleviate the detuning effect with a smaller TMD stroke.

ACKNOWLEDGEMENTS

The authors would like to thank the National Science Council of the Republic of China (Taiwan), for financially supporting this research under Contract No. NSC 100-2221-E-005-054.

REFERENCES

Chey, M. H., Chase, J. G., Mander, J. B, Carr, A. J. (2010). "Semi-active tuned mass damper building systems: Design," *Earthquake Engineering and Structural Dynamics*, 39(2), 119-139.

Chu, S. Y., Lin, C. C., Chung, L. L., Chang, C. C., Lu, K. H. (2008). "Optimal performance of discrete-time direct output feedback structural control with delayed control forces," *Structural Control and Health Monitoring*, 5(1), 20-42.

Lin, C. C., Hu, C. M., Wang, J. F., Hu, R. Y. (1994). "Vibration control effectiveness of passive tuned mass dampers. *Journal of the Chinese Institute of Engineers*," 17(3), 367-376.

Lin, C. C., Ueng, J. M., Huang, T. C. (2000). "Seismic response reduction of irregular buildings using passive tuned mass dampers," *Engineering Structures*, 22(5), 513-524.

Lin, C. C., Wang, J. F., Ueng, J. M. (2001). "Vibration control identification of seismically-excited MDOF structure-PTMD systems," *Journal of Sound and Vibration*, 240(1), 87-115.

Lu, L. Y., Lin, T. K., Yeh, S. W. (2010). "Experiment and analysis of a leverage-type stiffness controllable isolation system for seismic engineering," *Earthquake Engineering and Structural Dynamics*, 39(15), 1711-1736.

Lu, L. Y., Lin, G. L. (2009). "Improvement of near-fault seismic isolation using a resettable variable stiffness damper," *Engineering Structures*, 31(9), 2097-2114.

Nagarajaiah, S., Sonmez, E. (2007). "Structures with semi-active variable stiffness single/multiple tuned mass dampers," *Journal of Structural Engineering*, ASCE, 133(1), 67-77.

Yang, J. N., Kim, J. H., Agrawal, A. K. (2000). "Resetting semi-active stiffness damper for seismic response control," *Journal of Structural Engineering*, ASCE, 126(12), 1427-1433.